VIP Graphene Oxide Very Important Paper

DOI: 10.1002/anie.201404144

High Correlation between Oxidation Loci on Graphene Oxide**

Jinrong Yang, Guosheng Shi, Yusong Tu,* and Haiping Fang*

Abstract: *Recent experiments have shown the coexistence of both large unoxidized and oxidized regions on graphene oxide (GO), but the underlying mechanism for the formation of the GO atomic structure remains unknown. Now, using density functional calculations, 52 oxidation pathways for local pyrene structures on GO were identified, and a kinetic profile for graphene oxidation with a high correlation between oxidation loci was proposed, which is different from the conventional view, which entails a random distribution of oxidation loci. The high correlation is an essential nature of graphene oxidation processes and can be attributed to three crucial effects: 1) breaking of delocalized π bonds, 2) steric hindrance, and 3) hydrogen-bond formation. This high correlation leads to the coexistence of both large unoxidized and oxidized regions on GO. Interestingly, even in oxidized regions on GO, some small areas of sp^2-hybridized domains, similar to "islands", can persist because of steric effects.*

Through oxidation, pristine graphene becomes graphene oxide (GO), which bears oxidized functional groups.[1] This oxidation process significantly changes relevant electrical, mechanical, and thermal properties of GO.[1,2] For instance, in contrast to the hydrophobicity of graphene, GO has the vital advantage of water solubility; however, its surface does not become completely hydrophilic.[1b] GO may keep some properties that are characteristic of graphene, such as hydrophobicity, if the oxidized groups are not spread uniformly on the GO surface so that some unoxidized regions still exist. Therefore, it is of great importance for various potential applications of GO, such as in biosensors,[1b,3] next-generation optoelectronic nanodevices,[4] catalysis,[5] composites,[1b,6] and drug delivery, whether the oxidized parts are almost uniformly distributed or localized.[1a,7] Our own recent results have shown the existence of sufficiently large unoxidized regions on GO, how these regions are crucial to the antibacterial activity of the material,[8] and how they inhibit the growth of bacteria on the surface.[9] Furthermore, localized oxidized groups can have a great impact on the photoluminescence emission of GO[4a,10] and GO cutting processes.[11]

However, the precise chemical structure of GO remains to be elucidated, even though the GO structure has been studied for decades.[1b,12] To date, several models, the Hofmann–Holst,[12m] Ruess,[13] Scholz–Boehm,[14] Nakajima–Matsuoand,[15] Lerf–Klinowski,[12k,l] and Dékány[12i] models, have been successively proposed to depict the distribution of oxidized groups on GO. The most popular one, the Lerf–Klinowski model,[12e,l] depicts a GO layer as a random distribution of flat aromatic regions with unoxidized benzene rings and hydroxy and epoxy groups on the basal plane of the GO sheet.[12i] However, many recent experimental studies, which employed various observation methods, such as solid-state ^{13}C NMR spectroscopy,[16] transmission electron microscopy (TEM),[1b,12d,17] neutron diffraction,[18] X-ray absorption spectroscopy (XAS),[19] and scanning tunneling microscopy (STM),[20] have shown that large unoxidized graphene-like regions, which are separated by oxidized and functionalized regions, can exist in GO;[12d,16–18,20] these oxidized regions may contain some small patches of residual intact sp^2-hybridized domains, similar to "islands".[12d,17b,c,19] Cai et al. applied solid-state ^{13}C NMR spectroscopy to reveal in detail that a large fraction of the hydroxy and epoxy groups are found directly next to each other, and that sp^2-hybridized species are located in close proximity to each other.[16] Moreover, simulations for different GO phases have shown that the agglomeration of oxygen functional groups in dense islands is energetically favorable.[12b,21] For example, Yan et al. described the energetically favorable aggregation of hydroxy and epoxy groups for the formation of specific types of strips.[21e] In these studies, the starting point for studying the distribution of functional groups on GO was still based on the conventional view of randomly distributed oxidation loci. In fact, the underlying mechanism for the formation of the atomic structure and the coexistence of both unoxidized and oxidized regions remained unclear.

Herein, we identify 52 oxidation reaction pathways for local pyrene structures (including four hexagonal carbon rings) around oxidation loci and show a kinetic profile for graphene oxidation with high correlation between oxidation loci. This high correlation is a vital feature of graphene oxidation processes, and it can be attributed to three crucial factors: 1) breaking of delocalized π bonds, 2) steric hin-

[*] J.-R. Yang, Dr. G.-S. Shi, Prof. H.-P. Fang
Department Division of Interfacial Water and Key Laboratory of Interfacial Physics and Technology
Shanghai Institute of Applied Physics, Chinese Academy of Sciences
Shanghai 201800 (China)
E-mail: shiguosheng@sinap.ac.cn
J.-R. Yang
University of Chinese Academy of Sciences
Beijing, 100049 (China)
Dr. Y.-S. Tu
College of Physics Science and Technology, Yangzhou University, Jiangsu, 225009 and China Institute of Systems Biology, Shanghai University
Shanghai, 200444 (China)
E-mail: tuyusong@gmail.com

[**] This work is supported by NSFC (11290164 and 11105088), SNSFC (13ZR1447900), Shanghai University (HPC ZQ4000), the Supercomputer Center of the Chinese Academy of Sciences and the Shanghai Supercomputer Center of China. We thank Yi Gao and Pan Guo for helpful discussions and their crucial reading of this manuscript.

Supporting information for this article is available on the WWW under http://dx.doi.org/10.1002/anie.201404144.

drance, and 3) hydrogen-bond formation. The physical picture of graphene oxidation that we present is in accordance with recent experimental observations, which indicated the coexistence of both large unoxidized and oxidized regions and the occurrence of some small patches of sp^2-hybridized domains that may be viewed as islands in oxidized regions.

We combined density functional theory with conventional transition-state theory.[22] The B3LYP[23] functional was used to analyze the reaction mechanism of graphene oxidation by permanganate (MnO_4^-), and conventional transition-state theory was employed to analyze the rate constant of the oxidation reaction (for details, see the Supporting Information, PS1). For geometry optimization, the 6-31G(d) basis set was employed for O, C, and H atoms, and the LANL2DZ basis set was employed for Mn atoms. All calculations were performed using the Gaussian-09 package.[24]

Experimental and theoretical studies have shown that for oxidation processes of C=C bonds, the main oxidizing agent is MnO_4^-,[17b,25] and that the first step of the reaction of MnO_4^- with the C=C bond is the key and rate-limiting step.[25c,d,26] Considering that the oxidation reactions of MnO_4^- with both alkenes or graphene involve the breaking of C=C bonds, we here design processes of graphene oxidation by MnO_4^- to mimic the production of an intact GO sheet with two types of oxidized groups (−OH and −O−) on the surface by Hummers methods[27] (for more detailed discussions of the oxidant and graphene models, see PS2 and PS3). In fact, similar to the reaction of MnO_4^- to oxidize alkenes and their derivatives, we found that the first step of the oxidation of graphene with MnO_4^- is still the key and rate-limiting step, because graphene–MnO_4^- compounds can spontaneously decompose into MnO_3 and GO under the acidic reaction conditions (for a more detailed discussion, see the Supporting Information, PS2). Therefore, we herein considered only the formation of graphene–MnO_4^- compounds to be relevant for graphene oxidation. Figure 1a presents the relevant geometric structures of the reactants, the transition states, and the products of the oxidation of pure graphene with MnO_4^- (Path I), as an example, to show the oxidation reaction process. Considering the first- and second-neighbor sites around the oxidation loci, we designed 52 reaction pathways with different local pyrene structures on GO. The local pyrene structures are constituted

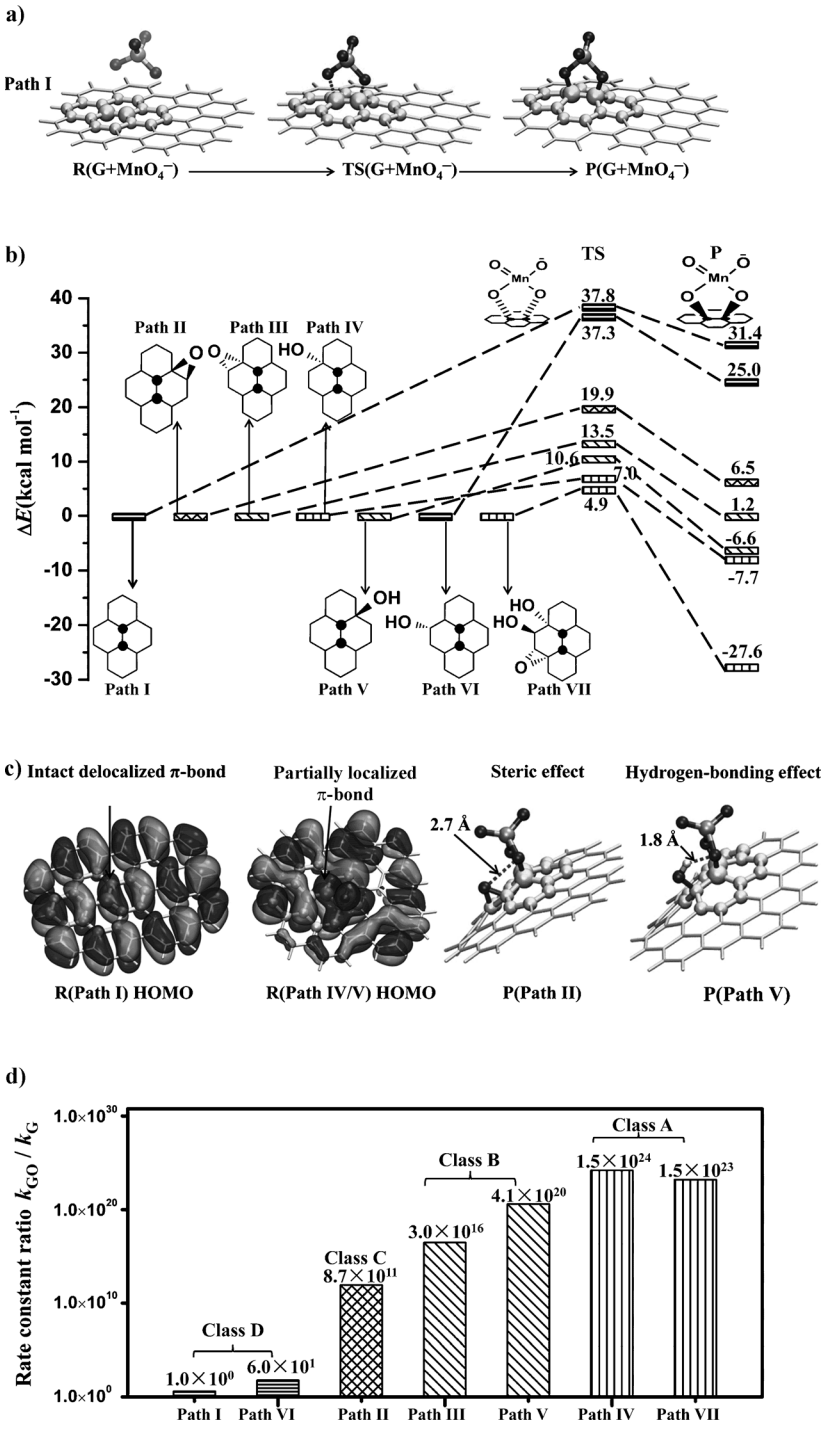

Figure 1. Oxidation processes of graphene by MnO_4^-. a) Relevant geometric structures of the reactants [R(G+MnO_4^-)], transition states [TS(G+MnO_4^-)], and products [P-(G+MnO_4^-)] for Path I. The graphene is shown by light grey lines, and the atoms in pyrene that are relevant to the reaction are shown as grey spheres (for MnO_4^-: oxygen black, manganese dark grey). A pair of neighboring carbon atoms at the oxidation loci are shown as large light grey spheres. b) Seven representative reaction pathways for the MnO_4^- oxidation process; ●: oxidation sites. c) Comparison of the highest occupied molecular orbitals (HOMO) of reactants R (Paths I and IV/V), the steric effect in Path II, and the hydrogen-bonding effect in Path V. The electron density was plotted for iso values of ±0.01 a.u. with black and grey denoting opposite signs. d) The rate-constant ratio k_{GO}/k_G of these representative GO oxidation reaction paths. k_{GO} and k_G are the rate constants for the oxidation of GO and graphene, respectively.

by a pair of intact neighboring carbon atoms, the oxidation loci, and the four six-membered aromatic rings that are attached to the two carbon atoms. Based on symmetry, approximately 181 types of neighbor sites exist around the oxidation loci (Figure 2; see also the Supporting Information, Figure S5).

Figure 1b presents seven representative reaction pathways for the MnO_4^- oxidation process, including the oxidation of the intact local arrangement (Path I), the graphene surface with pre-oxidized groups (epoxy or hydroxy) at the first-neighbor site of oxidation loci (Paths II–V), the graphene surface with pre-oxidized groups only at the second-neighbor sites of oxidation loci (Path VI), and the graphene surface both at the first- and second-neighbor sites of oxidation loci (Path VII). Whereas the reaction pathway in the presence of pre-oxidized groups at the first-neighbor site of oxidation loci (Path IV) entails an energy barrier of 7.0 kcal mol^{-1}, the energy barrier increases to 37.3 kcal mol^{-1} with pre-oxidized groups at the second-neighbor site (Path VI). This demonstrates that the impact of first-neighbor sites on the graphene oxidation process is significantly larger than that of second-neighbor sites, which highlights the most critical influence on the distribution of the oxidized groups on GO. The sites beyond the second-neighbor sites are nearly outside the hexagonal rings attached to the oxidation loci, and the impact on them can be ignored because in our calculations, the reaction energy barrier for pre-oxidized hydroxy groups at third-neighbor sites is much higher than that for first-neighbor sites (for more discussions, see Figure 2 and PS5).

Considering the impact from the local pyrene structure, which was described above in terms of neighboring sites, three significant factors influence the oxidation process: 1) breaking of delocalized π bonds, 2) steric hindrance, and 3) hydrogen-bond formation. For example, along Path IV, one carbon atom at the first neighboring site around the oxidation loci has been pre-oxidized to a C–OH structure. The delocalization of the π electrons on GO is broken in the pre-oxidized structure, and localized π bonds are obtained (Figure 1c). This breaking of the delocalized π bond substantially reduces the oxidation barrier.

Aside from the effect that is induced by π bond breaking, we also observed a steric-repulsion effect during the oxidation processes. The structure of Path II with one broken π bond is similar to that of Path III, but the reaction energy barrier of Path II is 6.4 kcal mol^{-1} larger than the barrier for Path III. This mainly lies in a steric-repulsion effect. When the oxidant (MnO_4^-) is located on the same side of the pre-oxidized epoxy species along Path II (see Figure 1c), the distance between the oxygen atom of the epoxy group and the oxygen atom of the oxidant (MnO_4^-) on the product [P(Path II)] is 2.7 Å shorter than the sum of two oxygen van der Waals radii (3.1 Å). Along Path III, however, the oxidant MnO_4^- is located on the opposite side of the pre-oxidized epoxy group. Therefore, the steric repulsion between the pre-oxidized group and the oxidant is much greater along Path II and increases its reaction energy barrier.

Interestingly, we observed an additional effect, the hydrogen-bonding effect (Figure 1c, the distance between the hydrogen atom of the hydroxy group and the oxygen atom of MnO_4^- on products [P(Path V)] is 1.8 Å). The hydrogen bond between the hydroxy (–OH) group and the oxidant can reduce the energy barrier of the reaction. For example, the barrier difference between Path V and Path IV is 2.8 kcal mol^{-1} smaller than the difference between Path II and Path III. Finally, the reaction along Path VII is influenced by a complicated combination of all three effects, and the barrier is only 4.9 kcal mol^{-1}.

From the above analysis, it becomes clear that the reaction barriers are dramatically lowered once the neighboring carbon atoms have been pre-oxidized and the relevant π bonds broken. The lower barriers lead to a larger probability that an oxidation reaction will occur. Thus, oxidation loci are highly correlated because of their neighboring positions. This high correlation between the oxidation loci agrees with recent experimental observations of isolated highly oxidized regions and large residual

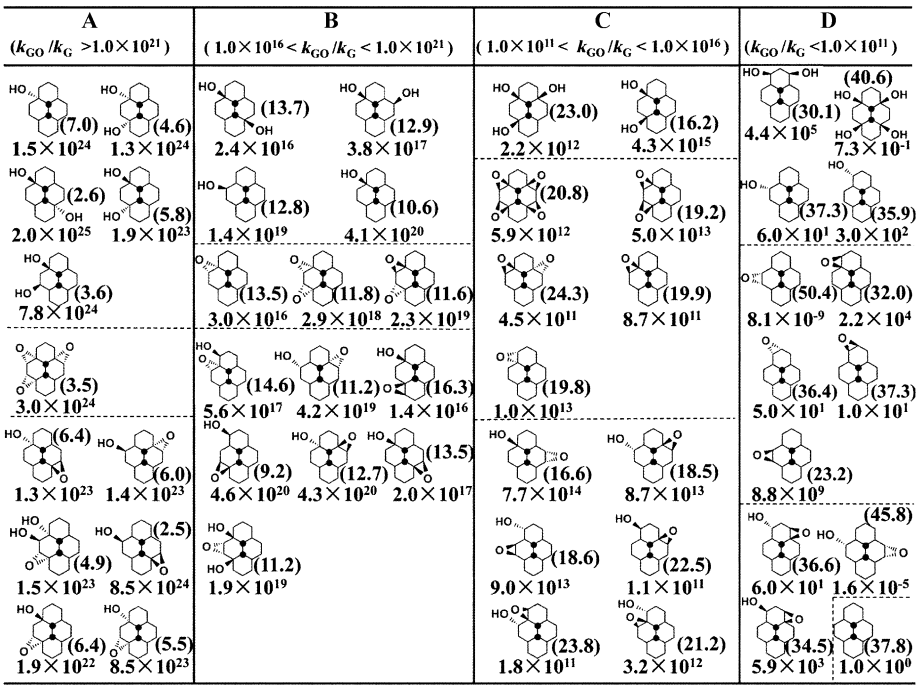

Figure 2. Rate-constant ratios for the local pyrene structures of 52 reaction paths. These paths are divided into four classes (A–D). The dotted lines separate the structures that contain only C–OH moieties, only C–O–C moieties, and C–OH moieties together with C–O–C moieties (from top to bottom). The values in brackets denote the reaction energy barrier (kcal mol^{-1}) of the 52 reaction paths for a local pyrene structure.

graphene-like sp^2 domains on GO.[1b,12d,16–20] From solid-state ^{13}C NMR spectroscopy, the strong intensity of one cross peak suggested that a large fraction of the sp^2-hybridized ^{13}C atoms are directly bonded to ^{13}C–OH and/or epoxide ^{13}C atoms, and another strong cross peak suggests that a large fraction of the C–OH and epoxide carbon atoms are bonded to each other.[16] These two cross peaks may indicate that the distribution of functional/oxidized groups should be highly correlated, which is consistent with our quantum computations.

Furthermore, we applied conventional transition-state theory[22] to analyze the rate constants of the oxidation reaction based on the reaction energy barriers (for details, see PS1). First, the rate constant k_G of the oxidation reaction of pristine graphene was taken as a basis for comparison; then the k_{GO}/k_G ratios of the oxidation reaction pathways for all local arrangements were calculated. We divided these rate-constant ratios into four categories (see Figure 1d): class A: $k_{GO}/k_G > 1.0\times10^{21}$ (including Paths IV and VII); class B: $1.0\times10^{16} < k_{GO}/k_G < 1.0\times10^{21}$ (Paths III and V); class C: $1.0\times10^{11} < k_{GO}/k_G < 1.0\times10^{16}$ (Path II); and class D: $k_{GO}/k_G < 1.0\times10^{11}$ (Paths I and IV). The k_{GO}/k_G ratios for all local configurations that correspond to the reaction paths identified here are listed in Figure 2. Obviously, the structures in class A feature pre-oxidized groups at first-neighbor sites; class A is the most crucial type and plays a decisive role in the formation of the oxidized-group distribution on GO during GO oxidation. The impacts of pre-oxidized groups at the second-neighbor sites belong to the structures in class D. Class B and C include synthetic configurations with pre-oxidized groups at first- and second-neighbor sites.

It should be interesting to explore the possible distribution of functional/oxidized groups on GO, as real oxidation processes in experiments are particularly complicated. We generated a possible evolution of graphene oxidation by permanganate (MnO_4^-), according to the rate-constant ratios for all local pyrene structures around the oxidation loci as listed in Figure 2 (see Figure S7 and PS6 for a Movie). During this evolution process, the high correlation between oxidation loci always led to the formation of localized regions with oxidized carbon rings; meanwhile, large areas of graphene remain unoxidized and intact. The coexistence of both unoxidized and oxidized regions is consistent with numerous similar observations in recent experiments. Ultrahigh-resolution TEM images of GO showed that interfaces exist between a large amount of pristine graphene regions and oxidized regions.[17c] It was also observed that upon oxidation, isolated highly oxidized areas (a few nanometers in size) are formed, while at least 60% of the surface remains undisturbed on oxidation.[17b] Interestingly, our evolution processes led to small patches of residual intact sp^2-hybridized domains, which may be viewed as islands in oxidized regions (Figure S7), which is also consistent with recently recorded TEM images.[12d,17b,c] The occurrence of these small patches can be attributed to the steric-repulsion effect on the oxidation process as described above. Meanwhile, hydrogen bonds can always be formed between neighboring oxide groups within the oxidized regions, and they partially reduce the energy barrier of the oxidation process and help stabilize the graphene oxide. Therefore, the distribution of oxide groups on GO should results from three effects: 1) breaking of delocalized π bonds, 2) steric hindrance, and 3) hydrogen-bond formation. Furthermore, we made numerical estimates of the correlation between oxidation loci to illustrate the contribution of the three crucial effects during graphene oxidation, and determined this correlation length to be 4.2 ± 0.5 nm. Interestingly, based on these correlations, the size of the patch islands can be estimated to be up to 0.65 ± 0.03 nm (for details, see PS5).

In summary, numerous calculations based on density functional theory and conventional transition-state theory on a series of local pyrene structures on GO show a kinetic profile with high correlation between oxidation loci on graphene oxide. We attribute this high correlation to three key factors: 1) breaking of delocalized π bonds, 2) steric hindrance, and 3) hydrogen-bond formation. This leads to the coexistence of both large unoxidized and oxidized regions. The correlation length is 4.2 ± 0.5 nm. Interestingly, the existence of the steric effect in oxidation reactions creates some small island-like patches of sp^2-hybridized domains, even within large oxidized regions. Based on these correlations, the size of the patch islands was estimated to be up to 0.65 ± 0.03 nm. Our study of the detailed atomic structure of GO not only provides new explanations for experimental observations and an extension of relevant molecular-dynamics studies, but also provides a more detailed description and understanding of the physical nature of the oxidized and unoxidized regions on GO.

Knowledge of the structure of these regions is of essential importance for understanding and using GO, as unoxidized regions retain characteristic features of graphene, such as hydrophobicity, and its electric and photonic properties. Such knowledge would also facilitate specific graphene functionalization processes with control over the atomic structure for various applications, including energy storage, optoelectronic devices, and biomedicine. Herein, we have reported the distribution characteristics of oxidized groups (epoxy and hydroxy groups) on an intact GO surface. The distribution of defects and carboxyl moieties (–COOH) around the GO edges as well as configuration adjustments of graphene–MnO_4^- compounds decomposing into different graphene oxides (with epoxy or hydroxy groups) after the oxidation reaction will be described in future work.

Received: April 9, 2014
Revised: May 14, 2014
Published online: July 13, 2014

Keywords: carbon · density functional calculations · graphene oxide · oxidation

[1] a) H. Y. Mao, S. Laurent, W. Chen, O. Akhavan, M. Imani, A. A. Ashkarran, M. Mahmoudi, *Chem. Rev.* **2013**, *113*, 3407–3424; b) D. Chen, H. Feng, J. Li, *Chem. Rev.* **2012**, *112*, 6027–6053.
[2] V. Georgakilas, M. Otyepka, A. B. Bourlinos, V. Chandra, N. Kim, K. C. Kemp, P. Hobza, R. Zboril, K. S. Kim, *Chem. Rev.* **2012**, *112*, 6156–6214.

[3] a) M. R. Karim, K. Hatakeyama, T. Matsui, H. Takehira, T. Taniguchi, M. Koinuma, Y. Matsumoto, T. Akutagawa, T. Nakamura, S.-i. Noro, T. Yamada, H. Kitagawa, S. Hayami, *J. Am. Chem. Soc.* **2013**, *135*, 8097 – 8100; b) S. S. Chou, M. De, J. Luo, V. M. Rotello, J. Huang, V. P. Dravid, *J. Am. Chem. Soc.* **2012**, *134*, 16725 – 16733; c) L. Jin, K. Yang, K. Yao, S. Zhang, H. Tao, S.-T. Lee, Z. Liu, R. Peng, *ACS Nano* **2012**, *6*, 4864 – 4875; d) E. Morales-Narváez, A. R. Hassan, A. Merkoçi, *Angew. Chem.* **2013**, *125*, 14024 – 14028; *Angew. Chem. Int. Ed.* **2013**, *52*, 13779 – 13783.

[4] a) P. V. Kumar, M. Bernardi, J. C. Grossman, *ACS Nano* **2013**, *7*, 1638 – 1645; b) A. L. Exarhos, M. E. Turk, J. M. Kikkawa, *Nano Lett.* **2013**, *13*, 344 – 349; c) P. Johari, V. B. Shenoy, *ACS Nano* **2011**, *5*, 7640 – 7647; d) K. P. Loh, Q. Bao, G. Eda, M. Chhowalla, *Nat. Chem.* **2010**, *2*, 1015 – 1024; e) K. Hu, L. S. Tolentino, D. D. Kulkarni, C. Ye, S. Kumar, V. V. Tsukruk, *Angew. Chem.* **2013**, *125*, 14029 – 14033; *Angew. Chem. Int. Ed.* **2013**, *52*, 13784 – 13788.

[5] a) C. Su, K. P. Loh, *Acc. Chem. Res.* **2013**, *46*, 2275 – 2285; b) C. Su, M. Acik, K. Takai, J. Lu, S.-j. Hao, Y. Zheng, P. Wu, Q. Bao, T. Enoki, Y. J. Chabal, K. P. Loh, *Nat. Commun.* **2012**, *3*, 1298; c) Q. Xiang, J. Yu, M. Jaroniec, *Chem. Soc. Rev.* **2012**, *41*, 782 – 796.

[6] a) J. Y. Kim, W. H. Lee, J. W. Suk, J. R. Potts, H. Chou, I. N. Kholmanov, R. D. Piner, J. Lee, D. Akinwande, R. S. Ruoff, *Adv. Mater.* **2013**, *25*, 2308 – 2313; b) X. Huang, X. Qi, F. Boey, H. Zhang, *Chem. Soc. Rev.* **2012**, *41*, 666 – 686; c) J. E. Kim, T. H. Han, S. H. Lee, J. Y. Kim, C. W. Ahn, J. M. Yun, S. O. Kim, *Angew. Chem.* **2011**, *123*, 3099 – 3103; *Angew. Chem. Int. Ed.* **2011**, *50*, 3043 – 3047.

[7] B. J. Hong, O. C. Compton, Z. An, I. Eryazici, S. T. Nguyen, *ACS Nano* **2012**, *6*, 63 – 73.

[8] Y. Tu, M. Lv, P. Xiu, T. Huynh, M. Zhang, M. Castelli, Z. Liu, Q. Huang, C. Fan, H. Fang, R. Zhou, *Nat. Nanotechnol.* **2013**, *8*, 594 – 601.

[9] F. Perreault, M. E. Tousley, M. Elimelech, *Environ. Sci. Technol. Lett.* **2014**, *1*, 71 – 76.

[10] J. Shang, L. Ma, J. Li, W. Ai, T. Yu, G. G. Gurzadyan, *Sci. Rep.* **2012**, *2*, 792.

[11] a) Z. Li, W. Zhang, Y. Luo, J. Yang, J. G. Hou, *J. Am. Chem. Soc.* **2009**, *131*, 6320 – 6321; b) L. Ma, J. Wang, F. Ding, *Angew. Chem.* **2012**, *124*, 1187 – 1190; *Angew. Chem. Int. Ed.* **2012**, *51*, 1161 – 1164; c) J.-L. Li, K. N. Kudin, M. J. McAllister, R. K. Prud′ homme, I. A. Aksay, R. Car, *Phys. Rev. Lett.* **2006**, *96*, 176101.

[12] a) J. E. Johns, M. C. Hersam, *Acc. Chem. Res.* **2013**, *46*, 77 – 86; b) S. Zhou, A. Bongiorno, *Sci. Rep.* **2013**, *3*, 2484; c) A. Hunt, D. A. Dikin, E. Z. Kurmaev, T. D. Boyko, P. Bazylewski, G. S. Chang, A. Moewes, *Adv. Funct. Mater.* **2012**, *22*, 3950 – 3957; d) D. Pacilé, J. Meyer, A. Fraile Rodríguez, M. Papagno, C. Gomez-Navarro, R. Sundaram, M. Burghard, K. Kern, C. Carbone, U. Kaiser, *Carbon* **2011**, *49*, 966 – 972; e) D. R. Dreyer, S. Park, C. W. Bielawski, R. S. Ruoff, *Chem. Soc. Rev.* **2010**, *39*, 228 – 240; f) S. Park, R. S. Ruoff, *Nat. Nanotechnol.* **2009**, *4*, 217 – 224; g) D. W. Boukhvalov, M. I. Katsnelson, *J. Am. Chem. Soc.* **2008**, *130*, 10697 – 10701; h) K. N. Kudin, B. Ozbas, H. C. Schniepp, R. K. Prud′Homme, I. A. Aksay, R. Car, *Nano Lett.* **2008**, *8*, 36 – 41; i) T. Szabó, O. Berkesi, P. Forgó, K. Josepovits, Y. Sanakis, D. Petridis, I. Dékány, *Chem. Mater.* **2006**, *18*, 2740 – 2749; j) G. Titelman, V. Gelman, S. Bron, R. Khalfin, Y. Cohen, H. Bianco-Peled, *Carbon* **2005**, *43*, 641 – 649; k) H. He, J. Klinowski, M. Forster, A. Lerf, *Chem. Phys. Lett.* **1998**, *287*, 53 – 56; l) A. Lerf, H. He, M. Forster, J. Klinowski, *J. Phys. Chem. B* **1998**, *102*, 4477 – 4482; m) U. Hofmann, R. Holst, *Ber. Dtsch. Chem. Ges.* **1939**, *72*, 754 – 771.

[13] G. Ruess, *Monatsh. Chem.* **1946**, *76*, 381 – 417.

[14] W. Scholz, H.-P. Boehm, *Z. Anorg. Allg. Chem.* **1969**, *369*, 327 – 340.

[15] T. Nakajima, Y. Matsuo, *Carbon* **1994**, *32*, 469 – 475.

[16] W. Cai, R. D. Piner, F. J. Stadermann, S. Park, M. A. Shaibat, Y. Ishii, D. Yang, A. Velamakanni, S. J. An, M. Stoller, J. An, D. Chen, R. S. Ruoff, *Science* **2008**, *321*, 1815 – 1817.

[17] a) J. C. Meyer, C. O. Girit, M. Crommie, A. Zettl, *Nature* **2008**, *454*, 319 – 322; b) C. Gómez-Navarro, J. C. Meyer, R. S. Sundaram, A. Chuvilin, S. Kurasch, M. Burghard, K. Kern, U. Kaiser, *Nano Lett.* **2010**, *10*, 1144 – 1148; c) K. Erickson, R. Erni, Z. Lee, N. Alem, W. Gannett, A. Zettl, *Adv. Mater.* **2010**, *22*, 4467 – 4472.

[18] J. Johnson, C. Benmore, S. Stankovich, R. Ruoff, *Carbon* **2009**, *47*, 2239 – 2243.

[19] S. Saxena, T. A. Tyson, E. Negusse, *J. Phys. Chem. Lett.* **2010**, *1*, 3433 – 3437.

[20] K. A. Mkhoyan, A. W. Contryman, J. Silcox, D. A. Stewart, G. Eda, C. Mattevi, S. Miller, M. Chhowalla, *Nano Lett.* **2009**, *9*, 1058 – 1063.

[21] a) B. Huang, H. Xiang, Q. Xu, S.-H. Wei, *Phys. Rev. Lett.* **2013**, *110*, 085501; b) M.-T. Nguyen, R. Erni, D. Passerone, *Phys. Rev. B* **2012**, *86*, 115406; c) N. Lu, D. Yin, Z. Li, J. Yang, *J. Phys. Chem. C* **2011**, *115*, 11991 – 11995; d) A. Bagri, C. Mattevi, M. Acik, Y. J. Chabal, M. Chhowalla, V. B. Shenoy, *Nat. Chem.* **2010**, *2*, 581 – 587; e) J.-A. Yan, L. Xian, M. Chou, *Phys. Rev. Lett.* **2009**, *103*, 086802.

[22] J. I. Steinfeld, J. S. Francisco, W. L. Hase, *Chemical kinetics and dynamics*, *Vol. 3*, Prentice Hall, Englewood Cliffs, **1989**.

[23] A. D. Becke, *J. Chem. Phys.* **1993**, *98*, 5648 – 5652.

[24] Gaussian 09 (Revision A.1), M. J. Frisch, et al., Gaussian, Inc., Wallingford, CT, **2009**.

[25] a) M. J. McAllister, J.-L. Li, D. H. Adamson, H. C. Schniepp, A. A. Abdala, J. Liu, M. Herrera-Alonso, D. L. Milius, R. Car, R. K. Prud′homme, I. A. Aksay, *Chem. Mater.* **2007**, *19*, 4396 – 4404; b) D. C. Marcano, D. V. Kosynkin, J. M. Berlin, A. Sinitskii, Z. Sun, A. Slesarev, L. B. Alemany, W. Lu, J. M. Tour, *ACS Nano* **2010**, *4*, 4806 – 4814; c) P. Adamczyk, A. Dybala-Defratyka, P. Paneth, *Environ. Sci. Technol.* **2011**, *45*, 3006 – 3011; d) S. Dash, S. Patel, B. K. Mishra, *Tetrahedron* **2009**, *65*, 707 – 739.

[26] a) C. H. A. Wong, C. K. Chua, B. Khezri, R. D. Webster, M. Pumera, *Angew. Chem.* **2013**, *125*, 8847 – 8850; *Angew. Chem. Int. Ed.* **2013**, *52*, 8685 – 8688; b) D. V. Kosynkin, A. L. Higginbotham, A. Sinitskii, J. R. Lomeda, A. Dimiev, B. K. Price, J. M. Tour, *Nature* **2009**, *458*, 872 – 876; c) R. Cruz-Silva, A. Morelos-Gomez, S. Vega-Diaz, F. Tristan-Lopez, A. L. Elias, N. Perea-Lopez, H. Muramatsu, T. Hayashi, K. Fujisawa, Y. A. Kim, M. Endo, M. Terrones, *ACS Nano* **2013**, *7*, 2192 – 2204.

[27] W. S. Hummers, Jr., R. E. Offeman, *J. Am. Chem. Soc.* **1958**, *80*, 1339.

